

The differential parameter method for multifrequency airborne resistivity mapping

Haoping Huang* and Douglas C. Fraser*

ABSTRACT

Helicopter EM resistivity mapping began to be accepted as a means of geologic mapping in the late 1970s. The data were first displayed as plan maps and images. Some 10 years later, sectional resistivity displays became available using the same "pseudolayer" half-space resistivity algorithm developed by Fraser and the new centroid depth algorithm developed by Sengpiel. Known as Sengpiel resistivity sections, these resistivity/depth images proved to be popular for the display of helicopter electromagnetic (EM) data in conductive environments.

A limitation of the above resistivity and depth algorithms is that the resulting Sengpiel section may imply that the depth of exploration of the EM system is substantially less than is actually the case. For example, a target at depth may be expressed in the raw data, but

its appearance on the Sengpiel section may be too shallow (which is a problem with the depth algorithm), or it may not even appear at all (which is a problem with the resistivity algorithm).

An algorithm has been adapted from a ground EM analytic method that yields a parameter called the differential resistivity, which is plotted at the differential depth. The technique yields the true resistivity when the half-space is homogeneous. It also tracks a dipping target with greater sensitivity and to greater depth than does the Sengpiel display method. The input parameters are the apparent resistivity and apparent depth from the pseudolayer half-space algorithm and the skin depth for the various frequencies. The output parameters are differential resistivity and differential depth, which are computed from pairs of adjacent frequencies.

INTRODUCTION

Airborne electromagnetic (EM) methods are being used increasingly as tools for geological mapping, groundwater exploration, and environmental mapping. In such helicopterborne applications, interpretation is commonly based on the mapping of apparent resistivity following the technique developed by Fraser (1978) using half-space models. The method was extended from a plan map display to a sectional display by Sengpiel (1988), who plotted the apparent resistivity ρ_a for each frequency at the so-called centroid depth z^* . More sophisticated methods, such as least-squares inversion to a layered earth based on singular value decomposition (Paterson and Reford, 1986), work well for noise-free data. However, these methods are seriously affected by leveling errors in the data, resulting in an unstable inversion (Palacky et al., 1992). They also are computationally intensive relative to half-space resistivity calculations. As a result, the popular and stable methods used in helicopter EM resistivity interpretation are

still based on the classical concept of the apparent resistivity of a half-space. Recent improvements in data quality, and an increase in the number of frequencies in airborne EM systems, encourage the search for new analytic methods for interpretation and data display.

A novel approach for the interpretation and display of multifrequency helicopter EM data is presented, which is based on the concepts of the apparent (half-space) resistivity and the effective depth. Of the five half-space models defined in Fraser (1978), we shall employ the pseudolayer half-space model that uses the inphase and quadrature signals, as calibrated in parts per million (ppm) of the primary field strength, to yield the apparent resistivity and apparent depth. The method described below uses this apparent resistivity and apparent depth as input parameters. It follows a technique developed for the analysis of MT and dipole EM ground data. It is similar in concept to that described by Macnae et al. (1991) for conductivity-depth imaging of airborne time-domain EM data. This new display method for airborne frequency

Presented at the Airborne Electromagnetics Workshop, Tucson, AZ, September 13-14, 1993. Manuscript received by the Editor June 10, 1994; revised manuscript received May 15, 1995.

*Dighem, a division of CGG Canada Ltd., 228 Matheson Blvd. E, Mississauga, Ontario L4Z 1X1, Canada.

© 1996 Society of Exploration Geophysicists. All rights reserved.

domain EM data is simple and yields a smoothed approximation of the true resistivity distribution with depth.

We are concerned here with the calculation of a resistivity parameter and the depth at which that parameter should be plotted.

RESISTIVITY AND DEPTH PARAMETERS

The depth parameter

We begin the calculation of the depth parameter by defining the effective depth z as a function of the skin depth δ and apparent depth da ,

$$z = f(\delta, da), \tag{1}$$

where $\delta = (\rho/\pi\mu_0 f)^{1/2}$ is the skin depth, da is the apparent depth to the top of the conductive half-space as obtained from the pseudolayer half-space algorithm of Fraser (1978), f is the frequency, μ_0 is the magnetic permeability of free space, and ρ is the resistivity of the ground. If the apparent resistivity ρ_a is substituted for the resistivity ρ , then the skin depth might more appropriately be referred to as the *apparent* skin depth, but this terminology is not used here.

In the case of an earth whose resistivity varies with depth, the apparent resistivity ρ_a from the half-space model represents a nonlinear averaging of the resistivities of all material above the effective depth and, indeed, some material below the effective depth. In general, however, the apparent resistivity ρ_{a_i} for a single frequency f_i can be represented approximately as (Bostick, 1977),

$$\rho_{a_i} \approx z_i / \int_0^{z_i} 1/\rho(z) dz, \tag{2}$$

where $\rho(z)$ is the resistivity of the ground as a function of depth, which is unknown in practice, and z_i is the effective depth determined from the i th frequency, as is indicated schematically in Figure 1. In practice, the apparent resistivity ρ_a is obtained from the pseudolayer half-space algorithm in Fraser (1978).

The difference between two effective depths, determined at two adjacent frequencies f_i and f_{i+1} , gives the thickness Δz for a hypothetical layer, i.e.,

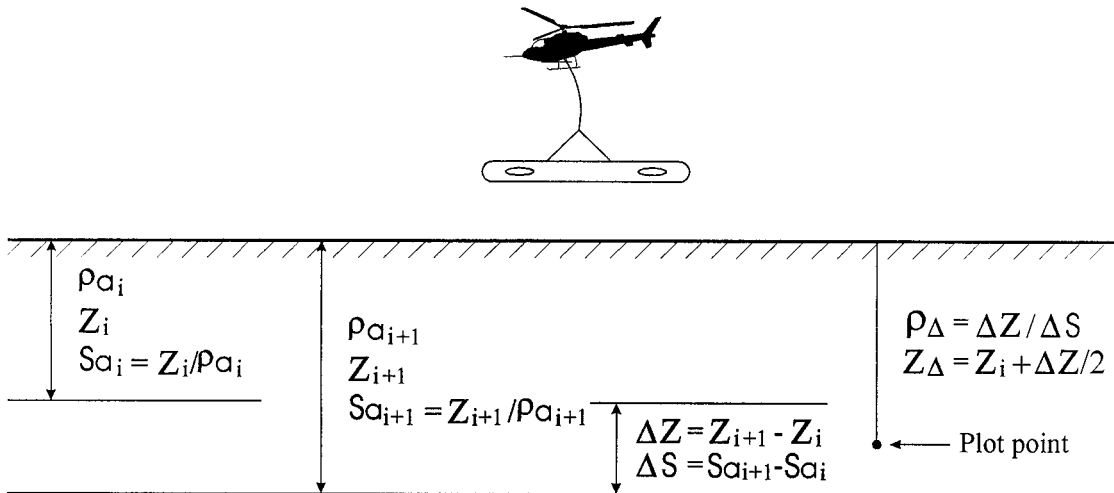
$$\Delta z = z_{i+1} - z_i = f(\delta_{i+1}, da_{i+1}) - f(\delta_i, da_i), \tag{3}$$

where the frequencies are in decreasing order, i.e., $f_{i+1} < f_i$. The depth to the midpoint of each hypothetical layer is called herein the differential depth and is given by Figure 1 as

$$z_\Delta = z_i + \Delta z/2 = (z_{i+1} + z_i)/2. \tag{4}$$

The differential depth z_Δ increases as the frequency decreases. This is the depth at which we plot the associated resistivity.

The effective depth of equation (1) was developed empirically and is displayed graphically in Figure 2. The goal of our development of the effective depth was to yield inputs to equations (3), (4), and (7) such that a resistivity/depth section would approximate the true resistivity distribution. With such a goal, various investigators could arrive at different relationships using a variety of input parameters, e.g., skin depth, apparent depth, or centroid depth. We have chosen the effective depth to be a function of the skin depth and the apparent depth. The apparent depth has some peculiar properties as described in Fraser (1978). For example, for a two-layer earth with a conductive upper layer, it is negative. Figure 2 provides a graphic presentation of the effective depth as a function of the skin depth (as calculated from the apparent resistivity) and the apparent depth. Since the effective depth is



ρ_a = apparent (half space) resistivity.
 $z = f$ (skin depth, apparent depth).

FIG. 1. The equivalent model where ρ_{a_i} and z_i are the apparent resistivity and effective depth, respectively, for frequency f_i ; Δz = thickness of hypothetical layer with a conductance ΔS ; and ρ_Δ = differential resistivity which is to be plotted at the differential depth z_Δ .

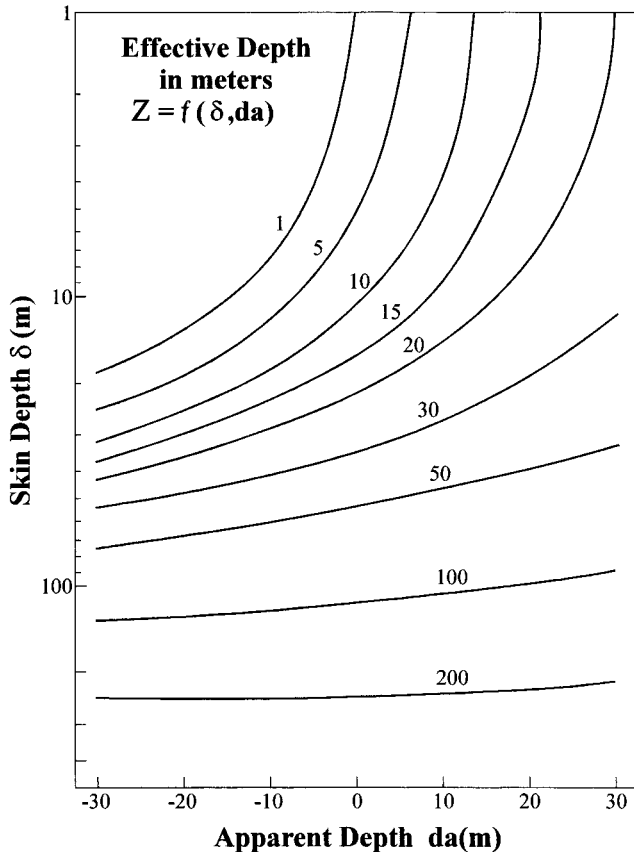


FIG. 2. The effective depth as a function of the skin depth and the apparent depth.

an empirical development, Figure 2 should be viewed as the current manifestation of this parameter which, in the future, may be altered to yield an improved resistivity/depth section.

The resistivity parameter

The apparent conductance Sa for a single frequency f_i refers to the ratio of the effective depth to the apparent resistivity, i.e., it is the sum of the conductances of the strata down to the effective depth. It can be written as

$$Sa_i = z_i / \rho_{a_i} \approx \int_0^{z_i} 1/\rho(z) dz. \tag{5}$$

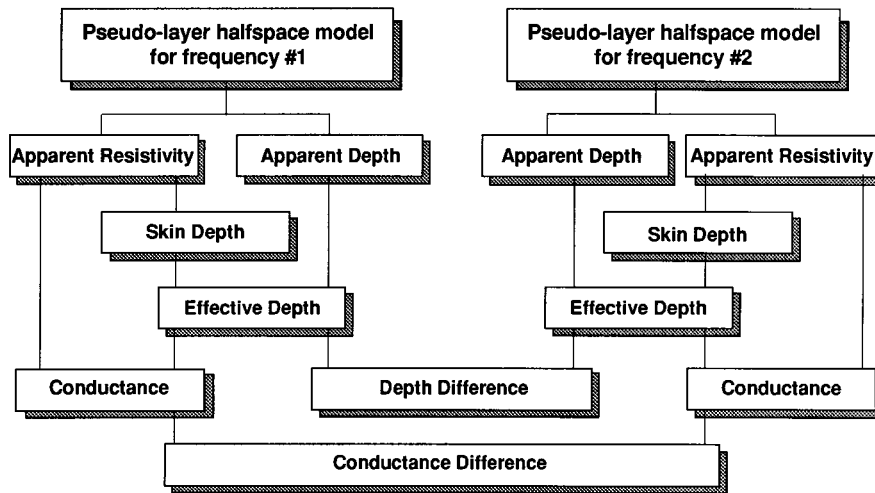
The difference between two apparent conductances, at two adjacent frequencies, gives the conductance for the hypothetical layer, i.e.,

$$\Delta S = Sa_{i+1} - Sa_i. \tag{6}$$

The differential resistivity may be approximated from the above parameters as,

$$\rho_{\Delta} = \Delta z / \Delta S. \tag{7}$$

Thus, if the apparent resistivities are known for a number of frequencies, equations (4) and (7) may be used to calculate a pair of resistivity and depth parameters ρ_{Δ} , z_{Δ} for each pair of adjacent frequencies. The procedure is summarized in Figure 3. By interpolation, the resistivity at intermediate depths can be obtained to yield a useful approximation of the true resistivity distribution. The resolution of the mapping of the resistivity in practice depends on the frequency band and



Differential resistivity = depth difference/conductance difference

Differential depth = effective depth (frequency #1) + 0.5 * depth difference

FIG. 3. The differential resistivity method uses the apparent resistivity and apparent depth obtained from the pseudolayer half-space model for a suite of frequencies. The method computes the conductances from the resistivities and depths, takes the conductance differences, and then recomputes the resistivities.

on the density of frequencies employed. The denser the frequencies and the wider the band, the higher the resolution.

MODEL TESTING

The approximate inversion technique described above is demonstrated below on some models of a layered earth, using 10 geometrically spaced frequencies in the range of 220 Hz to 115 000 Hz. These frequencies are transmitted by the coplanar coils of a helicopter EM system with an 8-m transmitter-receiver coil separation. The forward solutions to a layered earth are computed using a fast Hankel algorithm. These responses are inverted into the apparent resistivity of the equivalent half-space using the pseudolayer algorithm (Fraser, 1978) and the differential parameter method described above. All results are compared to the centroid depth approach developed in Sengpiel (1988).

Conductive cover

Figure 4 shows the results obtained for two flying heights over a two-layer earth representing the common situation of conductive overburden overlying a resistive basement. Curve ρ

is the true resistivity model, curve ρ_{Δ} is the differential resistivity versus the differential depth z_{Δ} , and curve ρ_a is the apparent resistivity versus the centroid depth z^* . Both the differential resistivity and the apparent resistivity increase with depth, indicating qualitatively that the lower layer is more resistive. Both of these resistivity parameters define the true resistivity of the upper layer, but not the true resistivity of the basement, for this particular case. The two main differences are, (1) the differential resistivity (solid circles) at the lowest frequency (greatest depth) is closer to the true resistivity of the model than is the apparent resistivity (open circles), and (2) the differential depth (solid circles) plots deeper into the basement than does the centroid depth (open circles). There is some dependency on flying height for both methods, although it is not serious in practice.

Resistive cover

Figure 5 shows the results for a model having a moderately resistive layer overlying a conductive basement. In this case, ρ_1 is well defined by both the Sengpiel and differential methods at the higher frequencies. When the differential depth approaches the layer interface for the lower frequencies, the differential

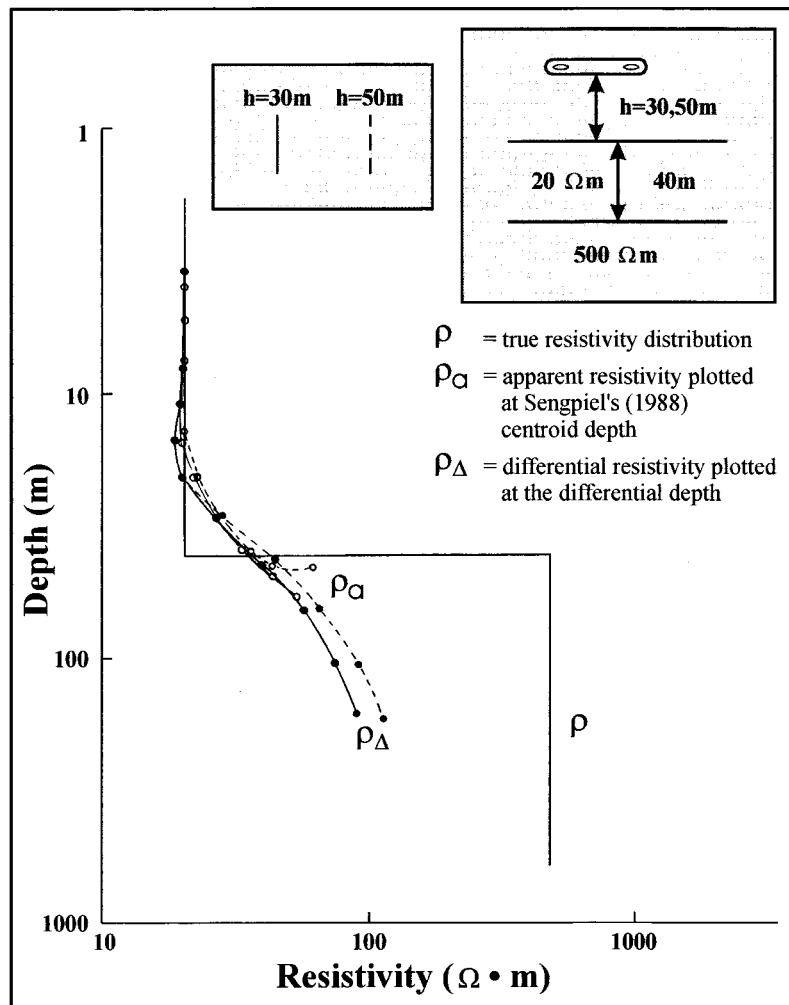


FIG. 4. Resistivity/depth diagram for two flying heights over a two-layer earth, where $\rho_1 = 20 \Omega \cdot m$, $\rho_2 = 500 \Omega \cdot m$, and $t_1 = 40 m$.

resistivity drops quickly to the correct ρ_2 value with only a negligible undershoot. The apparent resistivity, on the other hand, does not reach ρ_2 . The amount of the undershoot increases as the resistivity contrast between the two layers increases.

Four-layer model

The results for four-layer models are shown in Figures 6 and 7. The model for Figure 6a depicts a four-layer earth with resistivities of 50–1000–1–1000 ohm-m reflecting overburden on a resistive host containing a conductive target. The model for Figure 6b is the same as for Figure 6a, except for an increase in the thickness of the second layer. The curves for both the differential $\rho_{\Delta}(z_{\Delta})$ and the Sengpiel $\rho_{\beta}(z^*)$ methods indicate qualitatively that a four-layer earth exists. The differential curve $\rho_{\Delta}(z_{\Delta})$ rapidly follows the sharp changes in the resistivity at the layer interfaces, with the minimum value occurring close to the true depth of the thin conducting layer in Figures 6a and 6b. The differential resistivities in Figure 6 are closer to the true resistivities than are the apparent resistivities of the Sengpiel method.

Figure 6 as described above was computed using 10 geometrically spaced frequencies in the range of 220 Hz to 115 000 Hz. The

results for the same models, but using the five frequencies of a DIGHEM^V system (137 500, 27500, 5500, 1100, 220 Hz), are shown in Figure 7. The results are similar to Figure 6 but the resolution is poorer because of the sparser frequency sampling.

Dipping thin conductor

Figure 8 shows a 2-D model (upper panel) that is simulated by a series of multilayer 1-D models. There is an air layer shown in black that varies in thickness from about 10 m on the left to 0 m on the right. This air layer could represent a dense tree canopy where the altimeter defines the tree tops. There is patchy conductive overburden of 50 ohm-m, and a dipping conductive thin layer (5 m thick) of 1 ohm-m whose depth increases from about 20 m on the left to 200 m on the right. The host rock is 1000 ohm-m. The resistivity and depth values were calculated for the ten frequencies used in the earlier models and for a flying height of 30 m. The output color sections for the Sengpiel and differential methods are shown in the middle and lower panels, respectively, of Figure 8. It can be seen that the differential resistivity image reasonably approximates the true model shown in the upper panel, although these differential resistivities may be quite different from the true

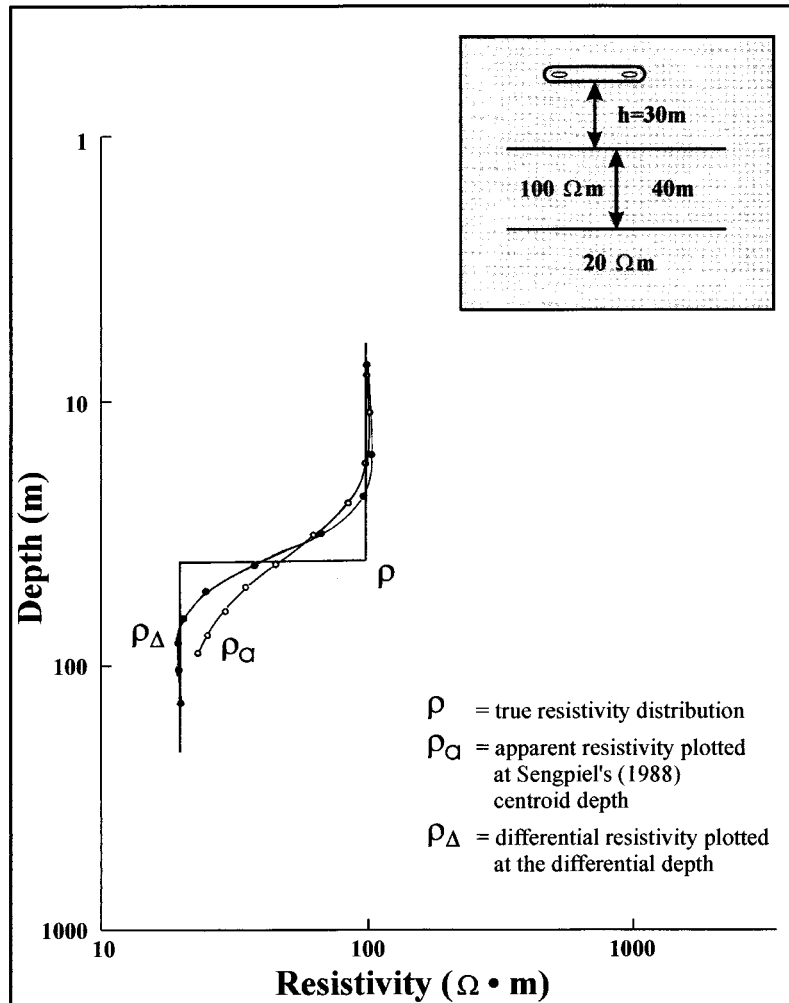


FIG. 5. Resistivity/depth diagram for a two-layer earth, where $\rho_1 = 100 \Omega \cdot m$, $\rho_2 = 20 \Omega \cdot m$, and $t_1 = 40$ m.

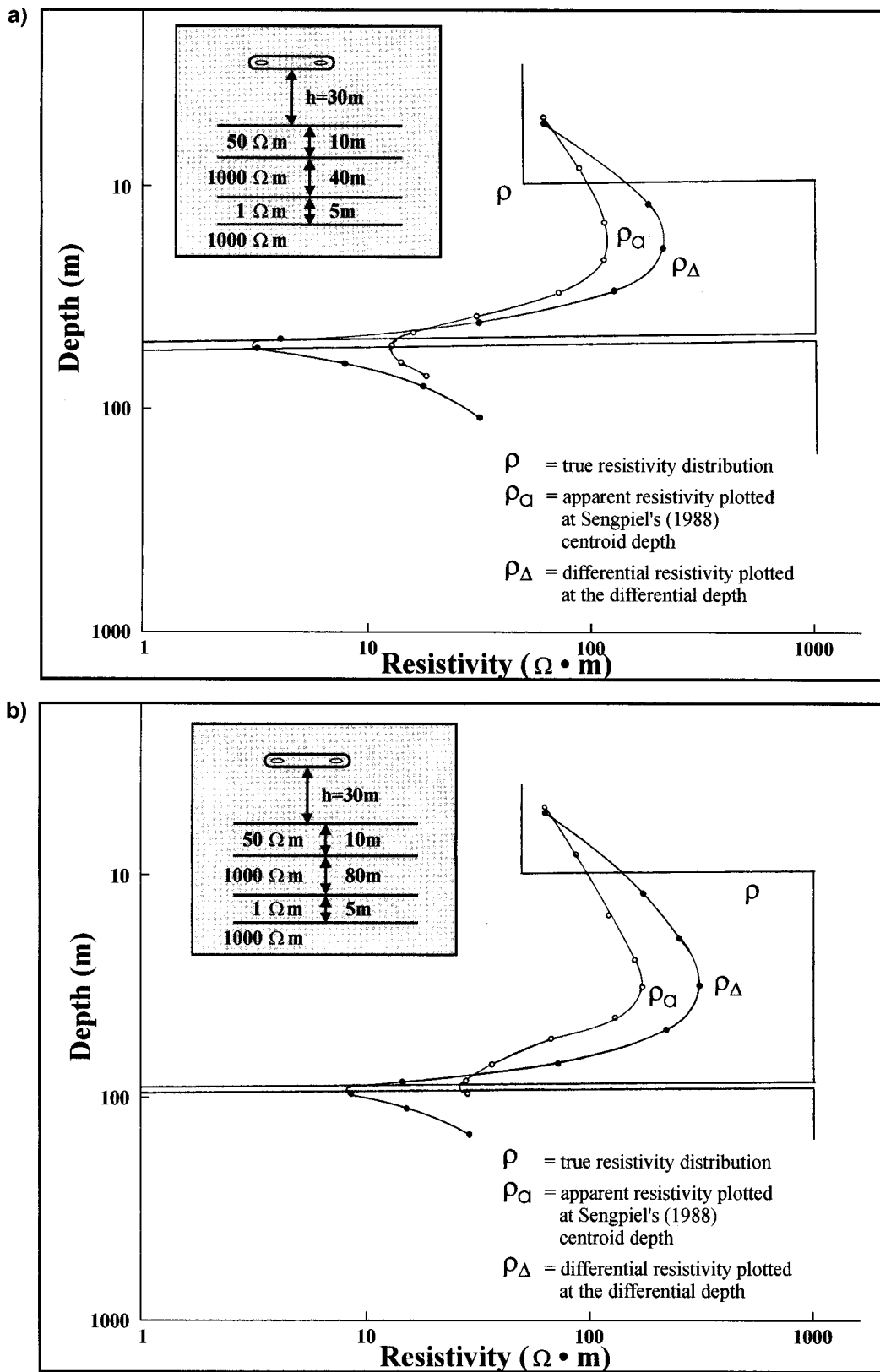


FIG. 6. Resistivity/depth diagram for a four-layer earth, where $\rho_1 = 50 \Omega \cdot m$, $\rho_2 = 1000 \Omega \cdot m$, $\rho_3 = 1 \Omega \cdot m$, $\rho_4 = 1000 \Omega \cdot m$, $t_1 = 10 m$, and $t_3 = 5 m$. (a) $t_2 = 40 m$ and (b) $t_2 = 80 m$.

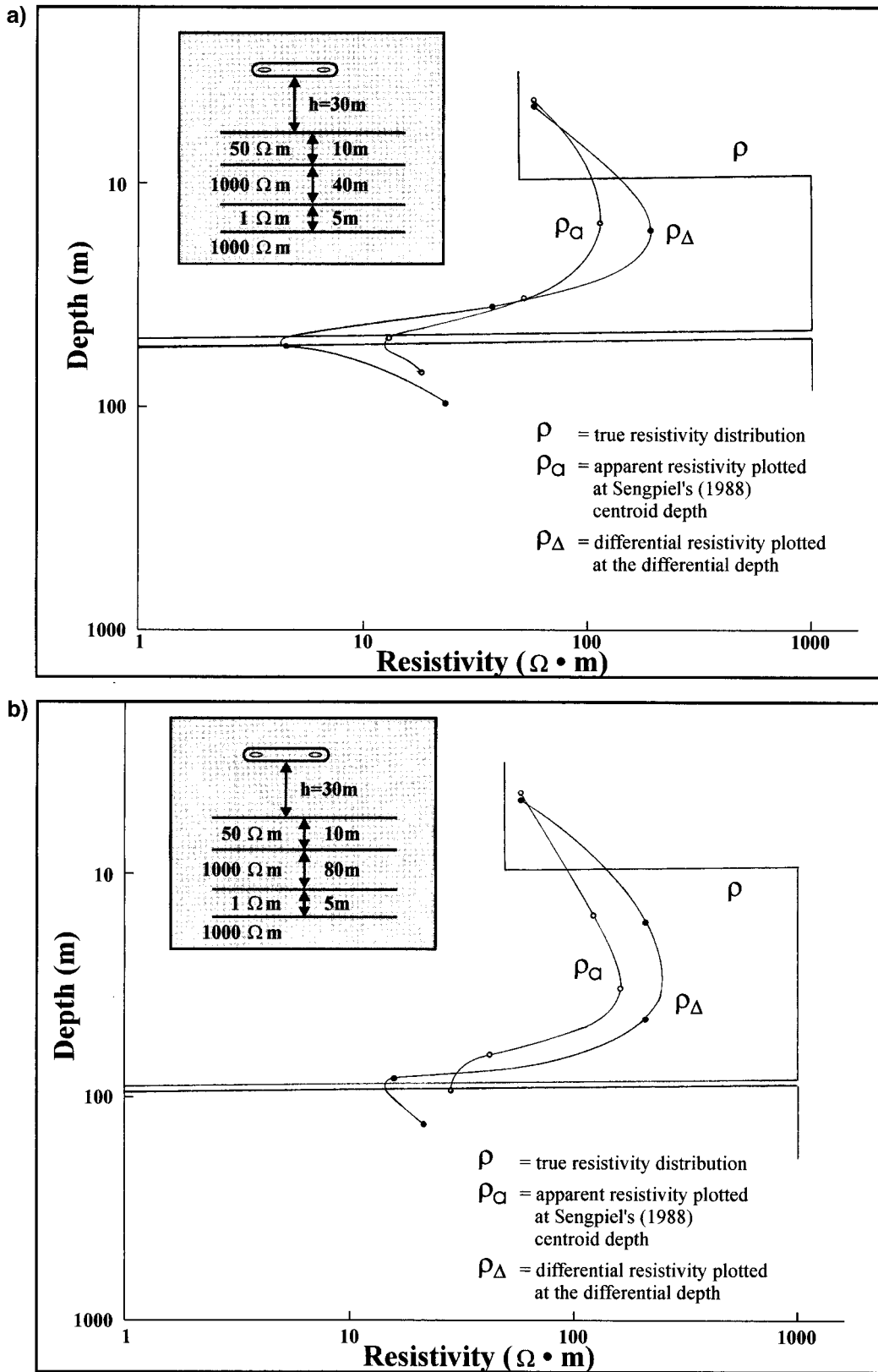


FIG. 7. Resistivity/depth diagram for the same model as Figure 6, but using 5 frequencies instead of 10. (a) $t_2 = 40$ m and (b) $t_2 = 80$ m.

resistivities. The moderately conductive upper layer is indicated on the differential section with a value that is close to the correct resistivity. The resistive second layer is reasonably defined, although its resistivity is understated. The conducting thin layer is well rendered although its resistivity is overstated. This dipping layer is visible on the differential section to a depth of 200 m for this noise-free data. The differential resistivity increases below the dipping layer, indicating that there is a resistive basement.

The center panel of Figure 8 presents an imaged Sengpiel section using the same color bar as for the differential image of

the lower panel. The layering of the model is indicated roughly in this image, giving a preliminary idea about the resistivity distribution. However, the image is not as definitive as that from the differential method of the lower panel. In particular, the appearance of the thin conducting layer is poorly rendered.

The above description of Figure 8 needs to be viewed qualitatively because the input data were generated from a series of horizontal multilayer 1-D models. Such models cannot accurately render the effect of the dip of the thin conductor or the lateral changes in resistivity caused by the patchy conductive overburden.

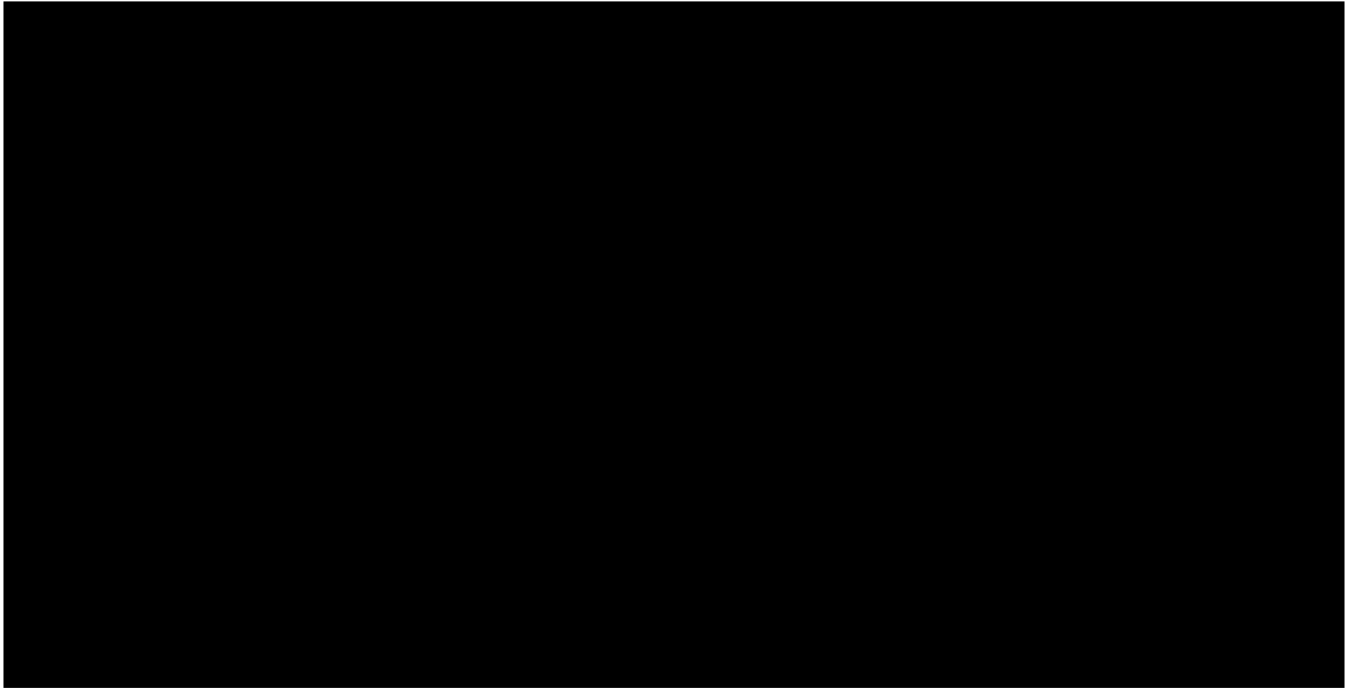


FIG. 8. Resistivity/depth section for a 2-D model (upper panel) simulated by a number of 1-D models. The center and lower panels are, respectively, the Sengpiel and differential sections.

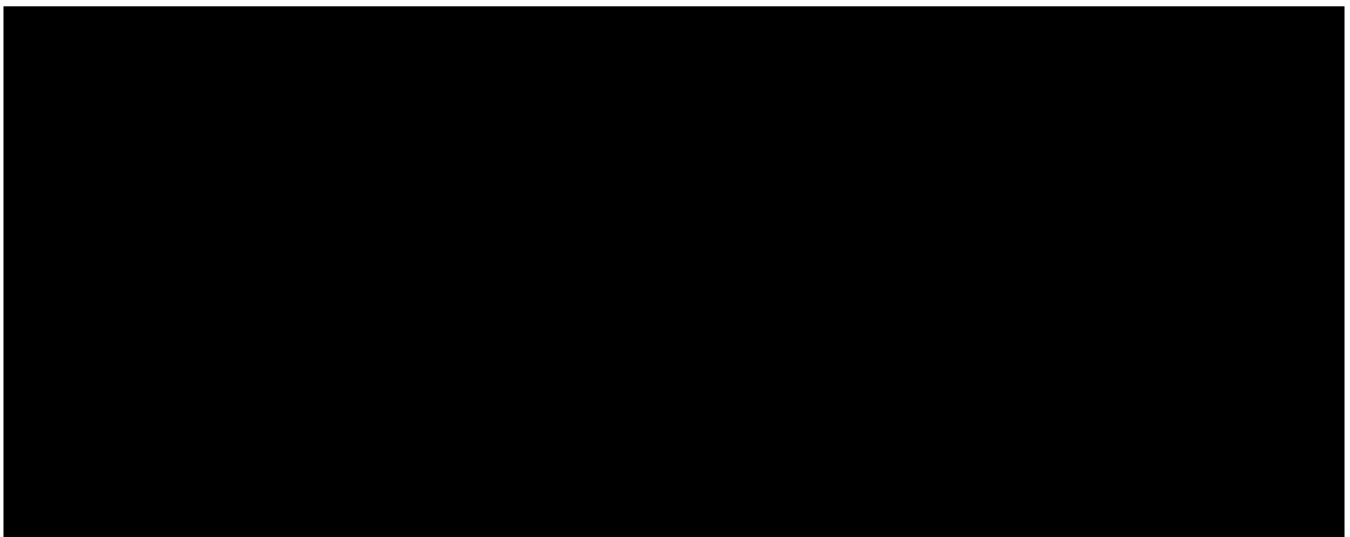


FIG. 9. Resistivity/depth section from three-frequency data obtained over the Cove gold deposit in Nevada. The upper and lower panels are, respectively, the Sengpiel and differential sections.

For a flying height of 30 m, and if minimal conductive overburden exists, Figure 8 suggests that it is possible to detect a conductive layer to a depth of 200 m when using the differential resistivity/depth method of sectional display. Tables 1 and 2 present the EM amplitudes in support of this statement.

A frequency of 900 Hz is common to all DIGHEM systems, and some DIGHEM^V systems employ 220 or 385 Hz as the lowest frequency. With noise levels of 1 to 2 ppm, it can be seen from the amplitudes of Table 2 versus Table 1 that a target layer is barely discernible at a depth of 200 m. Thus, 200 m could be referred to as the depth of exploration for this case when using the differential resistivity method.

FIELD EXAMPLE

The results of the differential and Sengpiel inversions of data from the Cove gold deposit in Nevada are shown in Figure 9. The Cove is a Carlin-type epithermal deposit that is located in the Augusta Mountain limestone formation south of Battle Mountain, Nevada. The gold and associated silver mineralization of the upper oxidized zone are associated with argillization (Emmons and Coyle, 1988), which yields a resistivity low.

The DIGHEM^{III} system was used in the Cove survey, operating at frequencies of 56000, 7200, and 900 Hz. The resistivity data were interpolated but not extrapolated to the surface or to a common depth. The Cove gold deposit is shown

as the steeply dipping red zone at the center of the sections. The red target zone and the more resistive rocks to its right are better defined on the differential resistivity section.

CONCLUSIONS

A technique has been developed for the approximate inversion of multifrequency helicopter EM measurements. The method is based on an apparent resistivity algorithm and the skin depth equation. The resistivity and depth are calculated directly, with the method tending to yield a smoothed approximation of the true resistivity distribution with depth. The algorithm is very efficient since the method does not employ an initial model, table matching, and iterative computations. Since the input values to the algorithm are the apparent resistivities, rather than the responses for a certain coil configuration, the apparent resistivities from a number of frequencies on both coplanar and coaxial coils can be used together. Mixing coaxial and coplanar coil orientations is permitted because the solution for the apparent resistivity is the same, provided both coil orientations have the same frequency and the superposed dipole assumption prevails (Fraser, 1979). The inversion improves with the number of frequencies because the function $\rho_{\Delta}(z_{\Delta})$ tends to be continuous. The output from this method could be used as an initial model for more sophisticated layered-earth inversions.

Table 1. Conductive cover (10 m of 50 ohm-m) overlies a resistive basement (1000 ohm-m). There is no conductive layer within the basement.

Frequency (Hz)	ppms		Sengpiel method		Differential method	
	Inphase	Quad	Apparent res. (ohm-m)	Centroid depth (m)	Diff. res. (ohm-m)	Diff. depth (m)
115200	1270.6	641.0	64	5	64	6
57600	884.9	711.5	87	8	169	13
28800	495.1	627.4	119	15	240	20
14400	224.6	447.3	160	25	320	33
7200	86.3	273.5	211	35	404	54
3600	29.6	152.1	267	45	470	87
1800	9.5	80.2	324	56	511	139
900	3.0	41.3	393	66	629	217
450	0.9	20.9	461	83	676	336
225	0.3	10.5	531	98	749	512

Table 2. Conductive cover (10 m of 50 ohm-m) overlies a resistive basement (1000 ohm-m). A horizontal conductive layer (5 m of 1 ohm-m) occurs with its top at a depth of 200 m.

Frequency (Hz)	ppms		Sengpiel method		Differential method	
	Inphase	Quad	Apparent res. (ohm-m)	Centroid depth (m)	Diff. res. (ohm-m)	Diff. depth (m)
115200	1270.6	641.0	64	5	64	6
57600	884.9	711.5	87	8	169	13
28800	495.1	627.5	119	15	240	20
14400	224.6	447.5	161	25	325	33
7200	85.5	272.3	213	35	416	54
3600	30.2	149.5	261	45	420	87
1800	12.2	78.0	258	52	255	130
900	6.7	40.6	189	56	91	172
450	4.3	21.8	120	73	38	207
225	2.5	12.2	84	97	37	246

The differential inversion technique was tested on synthetic, noise-free data from several models. The results were compared to the centroid depth method in Sengpiel (1988), which has become quite popular for the interpretation of helicopter frequency-domain EM data. The differential method yields images that are superior to those of the Sengpiel method. The differential inversion method was also tested on DIGHEM survey data from the Cove gold deposit in Nevada. It yielded a resistivity/depth section in which the gold deposit was well defined.

The differential resistivity technique is now being used routinely in the processing of DIGHEM survey data.

REFERENCES

- Bostick, Jr., F. X., 1977, A simple almost exact method of MT analysis, *in* Ward, S., Ed., Workshop on electrical methods in geothermal exploration: Univ. of Utah Res. Inst., U.S. Geol. Surv., Contract 14-08-0001-G-359, 174-183.
- Emmons, D. L., and Coyle, R. D., 1988, Echo Bay details exploration activities at its Cove gold deposit in Nevada: *Mining Eng.*, **40**, 791-794.
- Fraser, D. C., 1978, Resistivity mapping with an airborne multicoil electromagnetic system: *Geophysics*, **43**, 144-172.
- 1979, The multicoil II airborne electromagnetic system: *Geophysics*, **44**, 1367-1394.
- Macnae, J. C., Smith, R., Polzer, B. D., Lamontagne, Y., and Klinkert, P. S., 1991, Conductivity-depth imaging of airborne electromagnetic step-response data: *Geophysics*, **56**, 102-114.
- Palacky, G. J., Holladay, J. S., and Walker, P., 1992, Inversion of helicopter electromagnetic data along the Kapuskasing transect, Ontario: *in* Current Research, Part E, Geol. Surv. Canada, Paper 92-1E, 177-184.
- Paterson, N. R., and Reford, S. W., 1986, Inversion of airborne electromagnetic data for overburden mapping and groundwater exploration: *in* Airborne resistivity mapping, Palacky, G. J., Ed., Geol. Surv. Canada, Paper 86-22, 39-48.
- Sengpiel, K. P., 1988, Approximate inversion of airborne EM data from a multilayered ground: *Geophys. Prosp.*, **36**, 446-459.